CrystEngComm

PAPER

View Article Online
View Journal | View Issue

Cite this: *CrystEngComm*, 2018, **20**, 4194

Fluorogenic naked-eye sensing and live-cell imaging of cyanide by a hydrazine-functionalized CAU-10 metal–organic framework†

Rana Dalapati, [a] Soutick Nandi,[a] Helge Reinsch, [b] Bibhas K. Bhunia,[c] Biman B. Mandal, [c] Norbert Stock [b] and Shyam Biswas [*a]

A hydrazine-functionalized, highly stable Al(III) based metal–organic framework (MOF) with CAU-10 (CAU = Christian-Albrechts-University) framework topology namely CAU-10-N_2H_3 (**1**) was specifically designed to detect lethal CN^- ions in aqueous medium. The MOF was characterized by X-ray powder diffraction, infrared spectroscopy, gas sorption and thermogravimetric analyses. The isophthalate ligand in CAU-10 was functionalized by the hydrazine group to make the acidic –NH protons easily available to the CN^- ions. Indeed, the activated compound (**1′**) showed highly selective and sensitive responses to CN^- ions over other common anions with a detection limit of 0.48 μM. A rapid fluorescence enhancement was observed for **1′** with a large spectral shift ($\Delta\lambda$ = 30 nm) in the presence of CN^- ions in aqueous solution with the development of visible green fluorescence under a UV lamp. Due to the excellent detection performance to CN^- by **1′** in aqueous medium, the material was further used for CN^- detection in real water samples. The fluorescence increment with a large blue shift is attributed to the cyanide-induced deprotonation of the –NH group, which was confirmed by ^{1}H NMR titration measurements. The initial photo-induced electron transfer (PET) process is prohibited by this deprotonation, which causes the fluorescence enhancement. Time-resolved fluorescence lifetime measurements suggest that **1′** can also act as a lifetime based CN^- sensor. Finally, the CN^- sensing ability of **1′** inside living RAW 264.7 macrophages was demonstrated through live-cell imaging investigations.

Received 17th May 2018,
Accepted 21st June 2018

DOI: 10.1039/c8ce00818c

rsc.li/crystengcomm

Introduction

A large variety of fluorescent probes has been developed during the last twenty years for the sensing of anions. Among the common anions present in biological systems, the cyanide (CN^-) anion is deadly towards living organisms.[1] Cyanide-induced inhibition of respiration, which is caused by strong cyanide binding at the heme unit of cytochrome *c* in its active site, leads to cytotoxic hypoxia and cellular asphyxiation.[2] The WHO (World Health Organization) recommended that the tolerable concentration of cyanide for drinking water is only 1.9 μM.[3,4] Though a large number of fluorescent sensor materials have been investigated so far,[5] their applications for real biological or medical purposes require the use of a pure aqueous medium. Unfortunately, the majority of conventional organic fluorescent molecules work in a mixed-organic medium, which restricts their real-life applications.[6,7] The detection of cyanide by fluorescent sensors in 100% aqueous medium is still rare.[8,9] Hence, the development of new fluorescent sensors for CN^- ions, which can work in a pure aqueous system, is still a challenging work for environmental or medical applications.

A large number of inorganic and organic fluorescent compounds have been developed to date for detecting different types of species.[10,11] The combination of both inorganic and organic constituents makes the metal–organic framework (MOF) materials exceptional candidates in the area of fluorescence-based detection. Based on the great advantages of MOF materials, a large number of MOF materials have been examined as fluorescence-based sensors for gaseous, liquid and solid species.[12–15]

The main challenge of MOF materials for fluorescence sensing in an aqueous environment is their relatively low hydrolytic stability. Therefore, the smart design of water-stable MOFs is always desirable. Very recently, Ghosh *et al.* have

[a] *Department of Chemistry, Indian Institute of Technology Guwahati, 781039 Assam, India. E-mail: sbiswas@iitg.ernet.in; Fax: +91 3612582349; Tel: +91 3612583309*
[b] *Institut für Anorganische Chemie, Christian-Albrechts-Universität, Max-Eyth-Strasse 2, 24118 Kiel, Germany*
[c] *Biomaterial and Tissue Engineering Laboratory, Department of Biosciences and Bioengineering, Indian Institute of Technology Guwahati, Guwahati, 781039 Assam, India*

† Electronic supplementary information (ESI) available: NMR spectra, ESI-MS spectra, XRPD patterns, FT-IR spectra, TG curves, sorption isotherms and fluorescence spectra. See DOI: 10.1039/c8ce00818c

reported fluorescence-based cyanide sensing in aqueous medium by two MOF materials.[16,17] Unfortunately, for these systems, either post-synthetic modification of the ligand or encapsulation of a reactive fluorescent probe is required for the cyanide sensing. A simple, single-step synthesis procedure would be desirable over a multi-step method for the synthesis of the target MOF probe. To the best of our knowledge, only one report exists so far in the case of MOF materials, where post-synthetic modification or guest encapsulation is not required for the cyanide sensing.[18] Taking into account the above-mentioned concerns, in this work we present the preparation of a hydrazine-functionalized Al(III) MOF with CAU-10 (CAU = Christian-Albrechts-University) topology[19,20] called CAU-10-N_2H_3 (**1**). The activated (**1′**) material was employed for the fluorometric detection of lethal CN^- ions in pure aqueous medium. The MOF material shows fast response, good selectivity and sensitivity towards the detection of CN^- ions with naked-eye visualization of the green fluorescence under a UV lamp. The probe can also detect CN^- ions in water samples as well as in living cells.

Experimental section

Materials and physical measurements

All the reagent grade starting materials were obtained from commercial suppliers. Milli-Q water was used as a medium in all the fluorescence titration experiments. A Perkin Elmer Spectrum Two FT-IR spectrometer was used to record Fourier transform infrared spectra in the range of 440–4000 cm^{-1}. The following standard classifications were used to describe the FT-IR absorption bands: strong (s), medium (m), very strong (vs), broad (br), shoulder (sh) and weak (w). A Bruker D2 Phaser X-ray diffractometer working at 30 kV and 10 mA was utilized for the collection of X-ray powder diffraction (XRPD) patterns using Cu-Kα (λ = 1.5406 Å) radiation. A Mettler-Toledo TGA/SDTA 851e thermogravimetric analyzer was used to conduct thermogravimetric analyses in the temperature range of 25–600 °C with a heating rate of 5 °C min^{-1} under an air atmosphere. By employing a Quantachrome Autosorb iQ-MP gas sorption analyser, the nitrogen sorption experiments were accomplished at −196 °C, up to 1 bar. A Quantachrome iSorb-HP volumetric gas sorption analyser was applied for collecting the CO_2 adsorption isotherms (up to 1 bar) at 25 °C. Before the sorption analyses, the compounds were degassed at 100 °C overnight under dynamic vacuum. A HORIBA Jobin Yvon Fluoromax-4 spectrofluorometer was used to collect all the fluorescence emission spectra. To perform fluorescence lifetime measurements, an Edinburgh Instruments Life-Spec II instrument was employed, which utilizes the time-correlated single-photon counting method. The FAST software of Edinburgh Instruments was used for the fluorescence decay analysis by a reconvolution method.

Synthesis of the H_2IPA-N_2H_3 ligand

5-Aminoisophthalic acid (3.0 g, 0.016 mole) was suspended in 30 mL water/conc. HCl (2 : 1, v/v) mixture at 0 °C. An ice-cold solution (10 mL) of $NaNO_2$ (0.69 g, 0.01 mole) was added to it and the mixture was stirred for 30 min. Then, a solution of $SnCl_2{\cdot}2H_2O$ (6.77 g, 0.03 mole) in conc. HCl (20 mL) was added slowly with vigorous stirring and the reaction mixture was allowed to stir for an extra hour. The precipitate was filtered off, thoroughly washed with an excess amount of water and then dried at 60 °C in an oven for 6 h. The purification of the ligand was completed by column chromatography employing ethyl acetate as the eluent. Yield: 3.02 g (0.015 mole, 93%). ^{1}H NMR (δ, ppm, 600 MHz, DMSO-d_6): 8.76 (s, 1H, –NH), 8.05 (s, 1H, Ar–H), 7.77 (s, 2H, Ar–H). ^{13}C NMR (δ, ppm, 150 MHz, DMSO-d_6): 166.87, 146.70, 132.46, 123.06, 119.14. ESI-MS (m/z): 197.06 for $[M + H]^+$. The NMR and mass spectra are shown in Fig. S1–S3, ESI.†

Synthesis of $[Al(OH)(IPA\text{-}N_2H_3)]{\cdot}3.4H_2O{\cdot}0.5DMF$ (CAU-10-N_2H_3, 1)

For the synthesis of **1**, the H_2IPA-N_2H_3 ligand (0.20 g, 1.02 mmol), 2 M aqueous solution of $AlCl_3{\cdot}6H_2O$ (0.50 mL, 1.02 mmol), DMF (0.55 mL) and H_2O (1.75 mL) were mixed in a Teflon-liner and heated in a stainless steel autoclave at 120 °C for 12 h. The microcrystalline powder was filtered off and washed repeatedly with acetone (5 mL). Then, the solid was dispersed in water by sonication for 30 min. The dispersion was filtered and the light orange coloured solid was dried in an air oven at 80 °C for 6 h. Yield: 184 mg (0.77 mmol, 76%) based on the Al salt. Anal. cald. for $C_{9.5}H_{17.3}AlN_{2.5}O_{8.9}$ (335.93 g mol^{-1}): C, 33.96 H, 5.19 N, 10.42%. Found: C, 34.1 H, 4.9 N, 10.56%. FT-IR (KBr, cm^{-1}): 3419 (br), 3079 (w), 2923 (w), 2214 (w), 1684 (s), 1635 (s), 1577 (vs), 1434 (s), 1407 (vs), 1112 (m), 1004 (w), 785 (s), 727 (s), 607 (s), 526 (m).

Activation of the as-synthesized material

We activated the as-synthesized CAU-10-N_2H_3 material in two-steps. The stirring of the as-synthesized compound (200 mg) was conducted in methanol (50 mL) at ambient temperature for 24 h. Then, the solvent-exchanged compound was filtered off and degassed at 100 °C for 24 h under high vacuum. The activated form of **1** was denoted as **1′**.

Pawley refinement

The cell parameters were deduced by Pawley refinement using TOPAS software.[21] The model of CAU-10-N_2H_3 (activated form) was generated by force field optimization using the universal force field implemented in Materials Studio.[22] The structure of the structurally related compound CAU-10-N_3 was utilized as a preliminary model.[23] The cell parameters were changed to the ones observed for CAU-10-N_2H_3 (activated form) and the fractional position of the metal ions was fixed. The protons were generated using the implemented tool and the structural model was energetically optimized. However, no Rietveld refinement was possible which we attribute to the existence of solvent molecules within the pores and severe disorder in the structure induced by the bulky protic groups.

Fluorescence titration experiments

Initially, suspensions of **1′** in water having a concentration of 2 mg mL^{-1} were prepared by sonication to perform fluorescence titration measurements. Then, 100 μL of the suspension was diluted with 2900 μL of water (final concentration = 66.6 μg mL^{-1}) in a quartz cuvette and the solutions of different anions (concentration = 4 mM) were added in an incremental way.

Culture and maintenance of the RAW 264.7 (macrophage) cell line

RAW 264.7 macrophages (acquired from the National Centre for Cell Science, Pune, India) were cultured in high glucose Dulbecco's Modified Eagle's Medium (DMEM; Gibco, Life Technologies, U.S.A.) supplemented with 10% fetal bovine serum (FBS; Gibco, Life Technologies, U.S.A.) and 1% streptomycin–penicillin. Cells were seeded in a tissue culture flask and maintained at 37 °C in a humidified incubator with 5% CO_2. The medium was changed on every alternate day.

Cytocompatibility assay

Cytocompatibility of probe **1′** was checked by the MTT [3-(4,5-dimethylthiazol-2-yl)-2,5-diphenyltetrasodium bromide] (Sigma, U.S.A.) assay following a previously described protocol.[24] In brief, RAW 264.7 macrophages (5 × 103 cells in 180 μL) were plated in each well of a 96-well plate followed by the addition of 20 μL of different concentrations of probe **1′** (0–100 μM). The plates were kept for 72 h at 37 °C in a humidified incubator with 5% CO_2. After incubation, wells were replenished with fresh medium and 20 μL of MTT (prepared in a concentration of 5 mg ml^{-1} in phosphate buffered saline; PBS, pH = 7.4) was added in each well. 4 h of post incubation, 200 μL of dimethyl sulfoxide (DMSO; Sigma, U.S.A.) was added to solubilize the formazan crystals. Absorbance was recorded at 570 nm using a multiplate reader (Tecan Infinite 200 Pro, Switzerland).

Live cell imaging

For live cell imaging, RAW 264.7 macrophages (1 × 104 cells per well) were seeded in a 96-well plate and incubated at 37 °C in a humidified incubator with 5% CO_2. After 24 h, 25 μM of probe **1′** (prepared in the same cell culture media) was added and kept for 8 h. Post incubation, cells were washed with PBS (pH = 7.4) to remove surplus probe molecules from the surface of cells. Prior to live cell imaging, 15 μM of NaCN (prepared in PBS, pH = 7.4) was added to the wells and incubated for 15 min. However, few wells were left without addition of NaCN to understand the effect of only probe **1′**. Images were captured using a fluorescence microscope (EVOS FL, Life Technologies, U.S.A.).

Results and discussion

Synthesis and activation

The new hydrazine-functionalized MOF, CAU-10-N_2H_3 (**1**) was synthesized by following previous synthesis procedures documented for CAU-10-X (X = –H, –OCH_3, –CH_3, –NH_2, –NO_2, –OH) materials.[19,23] Briefly, a solvothermal reaction was conducted at 120 °C for 12 h between $AlCl_3{\cdot}6H_2O$ and the H_2IPA-N_2H_3 ligand with a 1 : 1 molar ratio using a mixed solvent system of *N*,*N*-dimethylformamide (DMF) and water. After the reaction, the microcrystalline powder material (**1**) was collected by filtration.

The solvent molecules entrapped in the pores of the as-synthesized compound (**1**) were first exchanged with methanol (having low boiling point and thus easily removable) molecules. Then, the solvent-exchanged **1** was heated under dynamic vacuum at 100 °C overnight to remove the guest solvent molecules. The solvent-exchange of the compound followed by thermal activation did not alter the XRPD pattern (Fig. S4, ESI†), which suggests that the compound retained its structural integrity throughout the activation process.

FT-IR spectroscopy

Both the as-synthesized and activated materials show very strong absorption bands around 1580 and 1405 cm^{-1} in their FT-IR spectra (Fig. S5, ESI†). These two absorption bands arise owing to the asymmetric and symmetric carboxylate stretching vibration of the framework IPA-N_2H_3 ligands, respectively.[25] In both IR spectra, the two sharp absorption bands around 785 and 725 cm^{-1} arise from the C–H out-of-plane vibrations of the hydrazine-functionalized ligand present in the framework structure.[26]

Structure description

The XRPD patterns of the as-synthesized and thermally activated samples of compound **1** were successfully indexed, which suggests that the compound crystallizes in the tetragonal crystal system possessing a space group of $I4_1/a$ (Table S1, ESI†). The Pawley refinement unveiled a good agreement between the assumed space group and the experimental XRPD patterns of **1** (Fig. 1 and S6, ESI†).

The isotypic crystal structure of CAU-10-N_3 was used as a preliminary model for the structural simulation by force-field calculation (for details, see Experimental section).[23] The framework structure of **1** is presented in Fig. 2. As revealed from the figure, the framework of CAU-10-N_2H_3 is formed by the interconnection of *cis*-corner sharing [AlO_6] octahedra with the hydrazine-functionalized isophthalate ligand molecules. This structural connectivity leads to the formation of helical chains (Fig. 3). Each helix is connected with four nearby inorganic building units having an alternating rotational arrangement through the coordinated isophthalate (IPA) ligands. Two adjacent helices are related by a mirror plane. This distinct arrangement of the inorganic building units and ligand molecules leads to the formation of square-shaped one-dimensional channels. The hydrazine functional groups protrude towards the inner side of these channels.

Thermal stability

Thermogravimetric analyses were carried out to check the thermal stability of the as-synthesized and activated materials

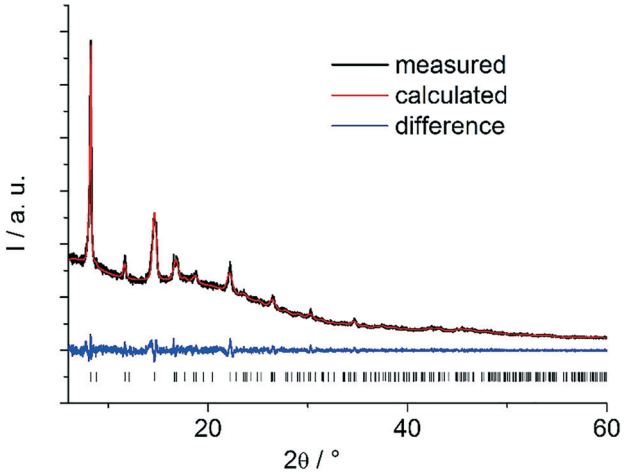

Fig. 1 Final Pawley refinement plot for as-synthesized **1**. The black and red curves denote the measured and calculated XRPD patterns, respectively. The difference between the experimental and theoretical data is indicated by the blue curve, whereas the allowed Bragg reflection positions are represented by vertical bars.

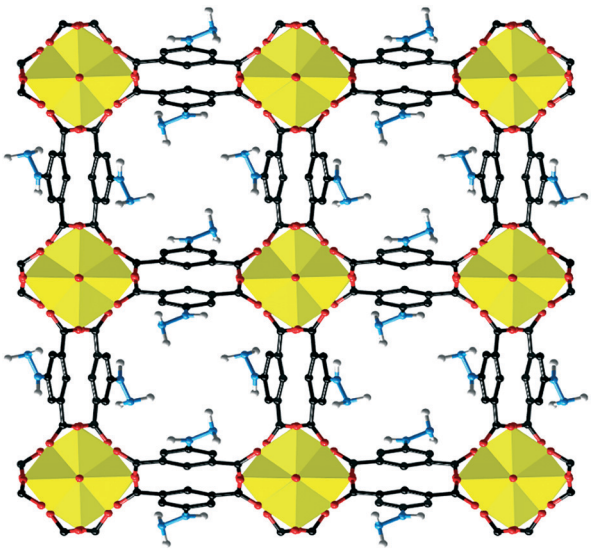

Fig. 2 The simulated structure of the framework of the CAU-10-N_2H_3 (**1**) compound. Colour codes: C, black; O, red; N, blue; Al, yellow polyhedra; H, white. Hydrogen atoms have been omitted from the phenyl ring of the structural diagram for clarity.

under an air atmosphere in the temperature range of 25–600 °C. TG curves of both forms of the material (Fig. S7, ESI†) reveal that the compound exhibits thermal stability only up to 250 °C. The structural collapse of the material occurs after this temperature due to the elimination of the coordinated IPA-N_2H_3 ligands from the framework.

The first weight loss of 18.4% in the TG curve of the as-synthesized compound in the range of 30–120 °C can be assigned to the elimination of 3.4 guest water molecules (calcd.: 18.2 wt%) per formula unit. In the second step, a weight loss of 10.6% in the temperature range of 130–190 °C can be ascribed to the removal of 0.5 DMF molecules per formula unit (calcd.: 10.8 wt%). The results of thermogravimetric and elemental analyses were utilized to determine the chemical formula of the CAU-10-N_2H_3 compound.

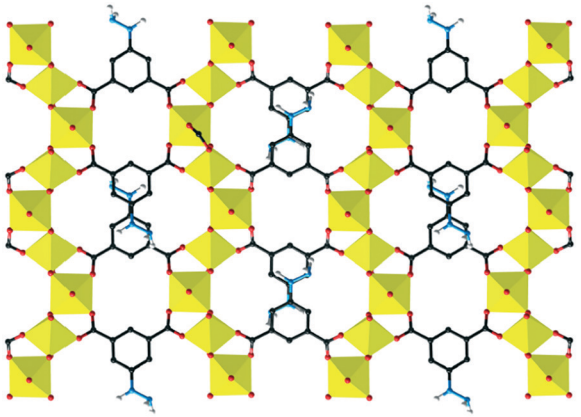

Fig. 3 Helical arrangement of [AlO_6] octahedra in the framework of CAU-10-N_2H_3 as seen along the *b*-axis. Colour codes: C, black; O, red; N, blue; Al, yellow polyhedra; H, white.

Gas sorption properties

The permanent porosity of the activated CAU-10-N_2H_3 material was checked by N_2 sorption analysis (Fig. S8, ESI†). The specific surface area (S_{BET}) of **1′** was calculated as 61 $m^2\ g^{-1}$ from the N_2 adsorption isotherm. Thus, the compound showed almost no porosity towards N_2, which contrasts with previously reported CAU-10-H (S_{BET} = 635 $m^2\ g^{-1}$) and CAU-10-NO_2 (S_{BET} = 440 $m^2\ g^{-1}$) materials.[27] We assume that the bulky hydrazine functional groups prohibit the free diffusion of N_2 molecules through the narrow channels.

A CO_2 adsorption experiment was additionally carried out to check the permanent porosity of **1′**. The low-pressure CO_2 adsorption measurement showed that the adsorption capacity reached up to 1.4 mmol g^{-1} (Fig. S9, ESI†) at 1 bar and 25 °C. Thus, the CO_2 adsorption experiment unambiguously verifies the permanent microporosity of activated **1**. The CO_2 adsorption capacity of **1′** is comparable with those of the existing structurally related CAU-10-X (X = –H, $–OCH_3$, $–CH_3$, $–NH_2$, $–NO_2$, –OH) compounds.[19]

Fluorescence intensity based sensing of CN^- ions

Due to the extreme toxicity of CN^- ions, a large number of fluorogenic probes have been developed in the past few decades for the sensing of CN^- ions.[16,28–30] Very recently, only a few MOF materials have been employed for the sensing of CN^- ions.[18] To check the hydrolytic stability of **1′**, we stirred the MOF material in water overnight. The recovered MOF material showed retention of its structural integrity after treatment with water, which was confirmed by the XRPD analysis (Fig. S10, ESI†). The non-toxicity and hydrolytic stability encouraged us to explore the applicability of the CAU-10-N_2H_3 material for the sensing of anions in pure aqueous medium.

Fluorescence titration experiments were carried out in order to serve this purpose. Thus, the emission spectra (λ_{ex} = 330 nm) of the stable aqueous suspension of **1′** were collected upon regular incremental addition of the sodium salts of different anions (Cl^-, I^-, F^-, Br^-, NO_3^-, NO_2^-, $H_2PO_4^-$, HSO_3^-, SO_4^{2-}, ClO_4^-, PO_4^{3-}, HSO_4^-, $S_2O_3^{2-}$, MeO^-, CN^- and SCN^-). Fig. 4 shows that a drastic enhancement in the fluorescence intensity with a large blue-shift ($\Delta\lambda$ = 30 nm) in the emission band was noticed only after the addition of the CN^- ion. Negligible changes in the fluorescence intensity were observed for all the other 15 potentially intrusive anions (Fig. 5 and S11, ESI†). These observations unequivocally support that the CAU-10-N_2H_3 probe is highly selective for CN^- ions over other common competing anions. Interestingly, the development of green fluorescence was observed after the addition of CN^- solution to the aqueous suspension of **1′**, which can be easily visualized by the naked eye under a normal UV-lamp. Furthermore, the XRPD pattern of **1′** was measured after the cyanide sensing experiment and no loss of crystallinity was observed (Fig. S12, ESI†). This observation confirms the structural integrity of the CAU-10-N_2H_3 material throughout the sensing event.

Time-dependent fluorescence investigations were carried out with different concentrations of CN^- ions in order to evaluate the response time of **1′** for the sensing of CN^- ions. We have monitored the fluorescence intensity of the CAU-10-N_2H_3 compound at a specific concentration of CN^- ions up to 15 min (Fig. S13, ESI†). The studies revealed that the compound showed a fast response time of approximately 2 min after the addition of CN^- solution.

For practical applications, it is desirable that the fluorescent probe should work effectively even in the presence of intrusive anions in complicated systems. To check the capability of the MOF material for the selective sensing of toxic CN^- ions, fluorescence titration experiments were carried out with **1′** after the addition of CN^- ions in the presence of other common interfering anions present in water. From Fig. 6 and S14–S28 (ESI†), it can be inferred that the detection ability of cyanide by **1′** was hardly influenced by the presence of other competitive anions. The relative fluorescence turn-on responses were found to be slightly lower with the co-existence of some anions like F^-, I^-, PO_4^{3-} and SO_4^{2-}. The F^-, PO_4^{3-} and SO_4^{2-} anions also have the affinity to form hydrogen bonding interactions with the acidic protons of receptor molecules.[31–33] Due to the competitive hydrogen bonding interactions, the relative fluorescence turn-on responses with the co-existence of these anions were found to be lower. On the other hand, the I^- ion is a well-known fluorescence quencher. The fluorescence quenching ability of the I^- ion is probably responsible for the comparatively lower fluorescence turn-on response. The outcomes of these fluorescence titration experiments substantiate that the hydrazine-functionalized MOF material exhibits an exceptional selectivity towards CN^- ions and the co-existence of other common anions does not significantly interfere with the selectivity.

The limit of detection (LOD) was calculated for this fluorogenic probe for CN^- ions. The LOD value was estimated to be 4.8×10^{-7} M (0.48 μM) (Fig. S29, ESI†) by using the following equation at a signal-to-noise ratio of 3:[34]

$$\mathrm{LOD} = 3\sigma/K$$

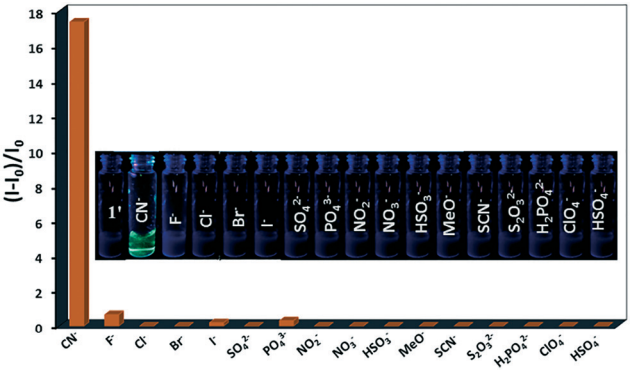

Fig. 5 Relative fluorescence enhancement behaviour of **1′** towards addition of different anions. Inset: naked-eye fluorogenic response of **1′** towards different anions.

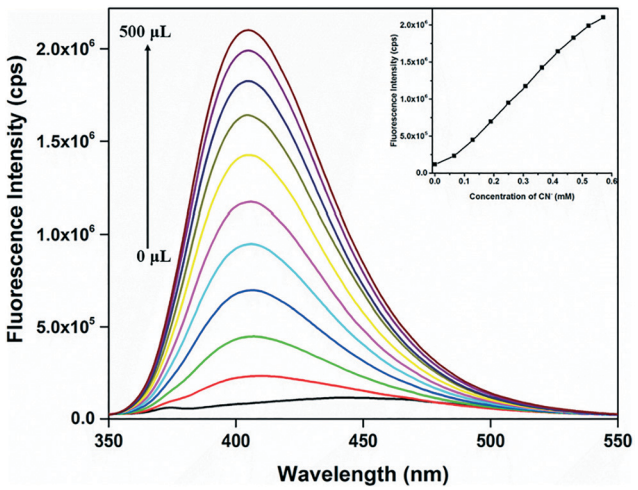

Fig. 4 Change in the fluorescence signal of **1′** with increasing addition of 4 mM CN^- solution. Inset: concentration-dependent fluorescence signal enhancement of **1′** monitored at 405 nm.

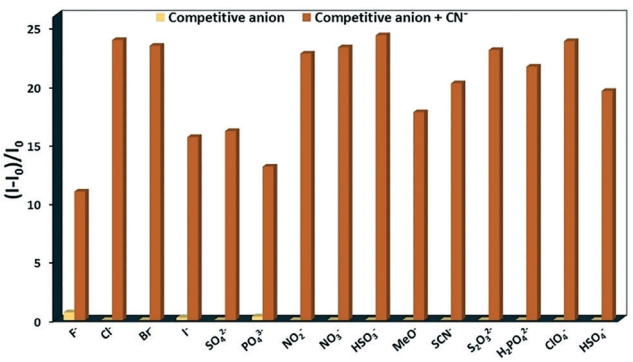

Fig. 6 Enhancement of the fluorescence signal of **1′** in the presence of an interfering anion, followed by the addition of CN^- solution.

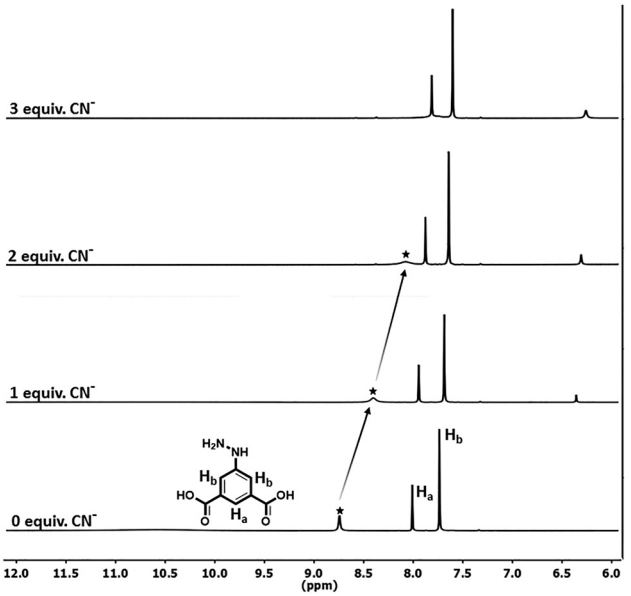

Fig. 7 Stacked ^{1}H NMR spectra of the H_2IPA-N_2H_3 ligand upon the addition of CN^- solution in DMSO-d_6 at 25 °C.

where σ indicates the standard deviation calculated from the initial intensity of the MOF material in the absence of CN^- solution and K stands for the slope of the linear curve which was obtained by plotting the fluorescence intensity of **1′** against the concentration of CN^- solution. The LOD value is lower than the World Health Organization (WHO) recommended concentration of CN^- ions in drinking water (2 μM).[35] The LOD value is comparable with those of the formerly reported fluorescent sensor materials (Table S2, ESI†). Hence, a MOF-based water monitoring system can be developed by using the presented hydrazine-functionalized MOF material.

Mechanism for the sensing of CN^- ions

The CN^- ion has the strong tendency to form hydrogen bonds with the acidic protons of sensor molecules.[36–38] Very recently, we have demonstrated that the deprotonation of the acidic –NH proton of a carbazole-functionalized Zr(IV) MOF by the CN^- ion can be utilized for the fluorescence turn-on sensing of the anion.[18] As a control experiment, unfunctionalized CAU-10-H MOF was treated with the CN^- ion. No obvious change in the fluorescence intensity was recorded for the CAU-10-H MOF (Fig. S30, ESI†). This result affirms that the hydrazine-functionalized ligand present in the MOF system is responsible for sensing. To check the possibility of the cyanide-induced deprotonation mechanism for the presented MOF probe, NMR titration experiments were conducted with the free H_2IPA-N_2H_3 ligand in DMSO-d_6 upon addition of the aqueous solution of the CN^- ion.[39] With increasing concentration of the CN^- ion, the intensity of the peak at 8.7 ppm for the –NH proton decreased gradually and shifted towards the up-field region of the spectrum (Fig. 7). After the addition of three equiv. of CN^- ion, the peak owing to the –NH proton disappeared, whereas a considerable up-field shift was observed for the peaks related to the aromatic protons. The disappearance of the peak due to the –NH proton and the drastic up-field shift of the corresponding peak affirm the cyanide-induced deprotonation of the –NH proton.

The cyanide induced deprotonation process can affect the electron transfer process throughout the MOF system. Initially, the photo-induced electron transfer (PET) process from the hydrazine moiety to the phenyl ring suppresses the fluorescence intensity of the MOF material. In the presence of the CN^- ion, the deprotonation-induced enhancement of the electron density throughout the framework prohibits the PET process, thus the fluorescence intensity of the MOF compound is enhanced. A similar fluorescence turn-on mechanism based on the inhibition of the electron transfer process has been proposed recently by Cao *et al.* for the selective detection of SO_2 gas by the amine-functionalized MOF-5.[40]

Fluorescence lifetime based sensing of CN^- ions

Time-resolved photoluminescence (TRPL) decay experiments were performed with **1′** to examine its excited-state behavior as well as feasibility to act as a lifetime-based sensor for CN^- ions. The TRPL decay profiles of the MOF probe were measured in the absence and presence of CN^- ions (Fig. S31, ESI†). The compound showed a bi-exponential decay curve with two species with an average excited-state lifetime of 0.38 ns (Table S3, ESI†). In the presence of the CN^- ion, the amplitude of the longer-lived component increased at the expense of the shorter-lived component and the average excited-state lifetime increased to 4.16 ns. The longer-lived species arises from the deprotonation of the –NH proton, which enhances the rate of radiative decay and consequently boosts the fluorescence intensity of the MOF material.[37,40,41] The noticeable change in the fluorescence intensity after cyanide addition points out that the implementation of a lifetime-based fluorescence sensor for toxic CN^- ions can be achieved by this MOF material.

Analysis of CN^- ions in real water samples

Encouraged by the excellent selectivity and sensitivity of **1′** towards CN^- sensing, we investigated the ability of the probe to detect CN^- ions in tap water and drinking water samples. Initially, no CN^- ion was found in either tap water or drinking water samples. Then, cyanide was spiked in the water

Table 1 Estimation of CN^- concentrations in real water samples

Water sample	CN^- spiked (μM)	CN^- found (μM)	Recovery (%)	RSD (%)
Tap water	10	9.7	97	2.1
	40	39.5	98.7	1.3
Drinking water	10	10.3	103	1.8
	40	40.6	101.5	1.2

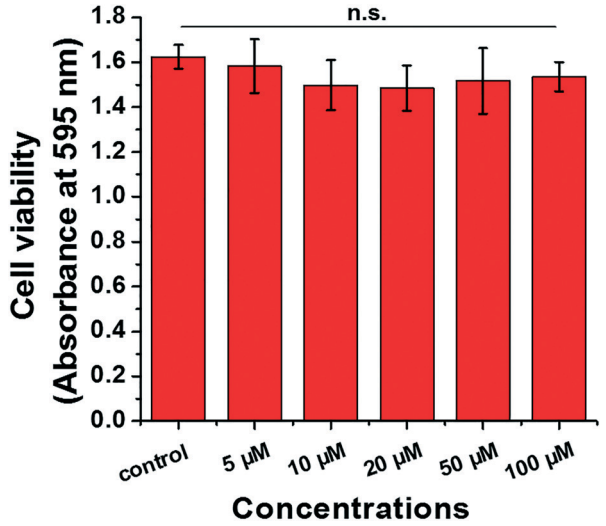

Fig. 8 Effect of different concentrations of 1′ on RAW 264.7 macrophages cultured in 96-well plates; data are represented as the average ± standard deviation, n = 3.

samples and the spiked samples were used for the fluorescence sensing experiments. The concentrations of CN^- ions in the water samples were determined from the linear curve which is shown in Fig. S28 (ESI†). The results obtained from these experiments are summarized in Table 1. The recovery for the cyanide sensing experiments ranges from 97.5 to 101.3% with very low RSD (n = 3; RSD = relative standard deviation) values, and suggests that 1′ has enormous potential for monitoring CN^- concentration in potable water.

Live-cell imaging of CN^- ions

A cellular imaging experiment was conducted to demonstrate the CN^- sensing ability of 1′ in living cells. To use the MOF probe for cell imaging, it must be biocompatible. Therefore, an *in vitro* cell viability test was carried out with RAW 264.7 cells. The cells were treated for 72 h with five varying concentrations (5–100 μM) of 1′. The data (shown in Fig. 8) demonstrated the cell viability as compared to the control sample (treated with PBS). The presence of 1′ had an almost negligible effect on cell viability. This cell viability experiment confirmed that the MOF probe 1′ is non-toxic to RAW 264.7 cells and it could be used for cell imaging investigation. As depicted in Fig. 9, the incubation of the RAW 264.7 cells with 1′ (25 μM) resulted in no fluorescence emission in the green fluorescence channel. In contrast, when the probe-loaded RAW 264.7 cells were treated with 15 μM CN^- solution, a bright green fluorescence signal was noticed. This observation is consistent with the results of the extracellular CN^- sensing experiment. From the results of live-cell imaging studies, it becomes inevitable that material 1′ can be used for monitoring cyanide toxicity inside the live cells.

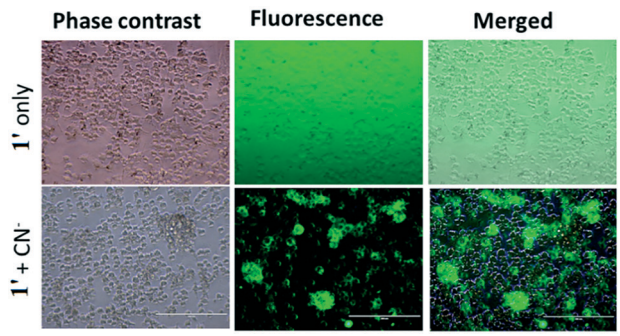

Fig. 9 Live cell imaging of CN^- by 1′. Phase contrast (first column), fluorescence (middle column) and merged images (third column) of 1′-loaded RAW 264.7 macrophages before (above row) and after (bottom row) incubation with 15 μM NaCN solution for 15 min at 37 °C. Scale bar = 200 μm.

Conclusions

In summary, we have shown the synthesis and systematic characterization of a hydrazine-functionalized Al(III) MOF namely CAU-10-N_2H_3 (1). The appropriate choice of a framework structure and functional group tethered with the ligand allowed us to utilize the material as a new sensor for the poisonous cyanide anion in aqueous medium. The activated material 1′ is capable of sensing CN^- ions even in the presence of other competitive anions present in water. The appearance of green fluorescence under UV light upon cyanide addition makes this material a naked-eye fluorescent sensor for CN^- ions in aqueous medium. The judicious design of a linker molecule with the acidic –NH proton facilitates the cyanide-induced deprotonation pathway, which leads to the fluorescence turn-on signal of the MOF probe. In addition, the fluorescence lifetime measurements indicate that material 1′ can also be used as a lifetime-based sensor for CN^- ions. The CAU-10-N_2H_3 probe shows a very low detection limit of 0.48 μM, which is lower than the allowable cyanide concentration (2 μM) in drinking water according to the WHO. Fascinated by the sensitive detection of CN^- ions in aqueous medium, we performed spike-and-recovery experiments, which confirm that compound 1′ has the capability to detect cyanide in environmental water samples. These results suggest that the CAU-10-N_2H_3 material can be used for controlling the quality of water samples. Furthermore, the live cell imaging experiments unambiguously demonstrate that probe 1′ is capable of sensing intracellular CN^- ions. Hence, the probe can be applied for monitoring cyanide toxicity in living cells.

Conflicts of interest

There are no conflicts to declare.

Acknowledgements

SB acknowledges the Science and Engineering Research Board (SERB), New Delhi (grant no. EEQ/2016/000012) for financial support. BBM is grateful to DST and DBT for providing financial assistance. Support for instrumental facility from the Central Instruments Facility (CIF) of IIT Guwahati is gratefully

acknowledged. We are thankful to the Ministry of Human Resource Development for funding the Center of Excellence in FAST (F. No. 5-7/2014-TS-VII).

Notes and references

1 K. N. Anjali, X. Shi, D. L. Harrison, J. E. Morningstar, S. Mahon, A. Chan, P. Sips, J. Lee, C. A. MacRae and G. R. Boss, *Cell Chem. Biol.*, 2017, **24**, 565–575.
2 F. Wang, L. Wang, X. Chen and J. Yoon, *Chem. Soc. Rev.*, 2014, **43**, 4312–4324.
3 W. H. Organization, *Guidelines for drinking-water quality*, World Health Organization, 2004.
4 H. L. Zhang, T. B. Wei, W. T. Li, W. J. Qu, Y. L. Leng, J. H. Zhang, Q. Lin, Y. M. Zhang and H. Yao, *Spectrochim. Acta, Part A*, 2017, **175**, 117–124.
5 J. Rocha, L. D. Carlos, F. A. A. Paz and D. Ananias, *Chem. Soc. Rev.*, 2011, **40**, 926–940.
6 T. Ebaston, G. Balamurugan and S. Velmathi, *Anal. Methods*, 2016, **8**, 6909–6915.
7 P. M. Reddy, S. R. Hsieh, C. J. Chang and J.-Y. Kang, *J. Hazard. Mater.*, 2017, **334**, 93–103.
8 Y. Y. Guo, X. L. Tang, F. P. Hou, J. Wu, W. Dou, W. W. Qin, J. X. Ru, G. L. Zhang, W. S. Liu and X. J. Yao, *Sens. Actuators, B*, 2013, **181**, 202–208.
9 E. Palomares, M. V. Martínez-Díaz, T. Torres and E. Coronado, *Adv. Funct. Mater.*, 2006, **16**, 1166–1170.
10 L. Basabe-Desmonts, D. N. Reinhoudt and M. Crego-Calama, *Chem. Soc. Rev.*, 2007, **36**, 993–1017.
11 S. M. Ng, M. Koneswaran and R. Narayanaswamy, *RSC Adv.*, 2016, **6**, 21624–21661.
12 L. E. Kreno, K. Leong, O. K. Farha, M. Allendorf, R. P. V. Duyne and J. T. Hupp, *Chem. Rev.*, 2011, **112**, 1105–1125.
13 L. Guo, M. Wang and D. Cao, *Small*, 2018, **14**, 1703822.
14 M. Wang, L. Guo and D. Cao, *Sens. Actuators, B*, 2018, **256**, 839–845.
15 Z. Xiang, C. Fang, S. Leng and D. Cao, *J. Mater. Chem. A*, 2014, **2**, 7662–7665.
16 A. Karmakar, N. Kumar, P. Samanta, A. V. Desai and S. K. Ghosh, *Chem. – Eur. J.*, 2016, **22**, 864–868.
17 A. Karmakar, B. Joarder, A. Mallick, P. Samanta, A. V. Desai, S. Basu and S. K. Ghosh, *Chem. Commun.*, 2017, **53**, 1253–1256.
18 A. Das and S. Biswas, *Sens. Actuators, B*, 2017, **250**, 121–131.
19 H. Reinsch, M. A. v. d. Veen, B. Gil, B. Marszalek, T. Verbiest, D. D. Vos and N. Stock, *Chem. Mater.*, 2012, **25**, 17–26.
20 H. Jin, A. Wollbrink, R. Yao, Y. Li, J. Caro and W. Yang, *J. Membr. Sci.*, 2016, **513**, 40–46.
21 A. Coelho, *Topas Academics 4.2*, Coelho Software, Brisbane, 2007.
22 *Materials Studio Version 5.0*, Accelrys Inc., San Diego, 2009.
23 S. Nandi, H. Reinsch, S. Banesh, N. Stock, V. Trivedi and S. Biswas, *Dalton Trans.*, 2017, **46**, 12856–12864.
24 J. P. Kumar, R. Konwarh, M. Kumar, A. Gangrade and B. B. Mandal, *ACS Sustainable Chem. Eng.*, 2018, **6**, 1235–1245.
25 N. R. Dhumal, M. P. Singh, J. A. Anderson, J. Kiefer and H. J. Kim, *J. Phys. Chem. C*, 2016, **120**, 3295–3304.
26 H. Reinsch, S. Waitschat and N. Stock, *Dalton Trans.*, 2013, **42**, 4840–4847.
27 D. Fröhlich, S. K. Henninger and C. Janiak, *Dalton Trans.*, 2014, **43**, 15300–15304.
28 Y. Kim, H. S. Huh, M. H. Lee, I. L. Lenov, H. Zhao and F. P. Gabbaï, *Chem. – Eur. J.*, 2011, **17**, 2057–2062.
29 N. Busschaert, C. Caltagirone, W. V. Rossom and P. A. Gale, *Chem. Rev.*, 2015, **115**, 8038–8155.
30 A. K. Mahapatra, K. Maiti, S. K. Manna, R. Maji, C. D. Mukhopadhyay, B. Pakhira and S. Sarkar, *Chem. – Asian J.*, 2014, **9**, 3623–3632.
31 B. Sui, B. Kim, Y. Zhang, A. Frazer and K. D. Belfield, *ACS Appl. Mater. Interfaces*, 2013, **5**, 2920–2923.
32 R. Dalapati and S. Biswas, *Sens. Actuators, B*, 2017, **239**, 759–767.
33 S. D. Padghan, R. S. Bhosale, N. V. Ghule, A. L. Puyad, S. V. Bhosale and S. V. Bhosale, *RSC Adv.*, 2016, **6**, 34376–34380.
34 L. Long, L. Wang, Y. Wu, A. Gong, Z. Da, C. Zhang and Z. Han, *Chem. – Asian J.*, 2014, **9**, 3291–3298.
35 M. La, Y. Hao, Z. Wang, G.-C. Han and L. Qu, *J. Anal. Methods Chem.*, 2016, **2016**, 1462013.
36 J. Jo and D. Lee, *J. Am. Chem. Soc.*, 2009, **131**, 16283–16291.
37 S. Saha, A. Ghosh, P. Mahato, S. Mishra, S. K. Mishra, E. Suresh, S. Das and A. Das, *Org. Lett.*, 2010, **12**, 3406–3409.
38 C. Zhang, C. Liu, B. Li, J. Chen, H. Zhang, Z. Hu and F. Yi, *New J. Chem.*, 2015, **39**, 1968–1973.
39 R. Chutia, S. K. Dey and G. Das, *Cryst. Growth Des.*, 2015, **15**, 4993–5001.
40 M. Wang, L. Guo and D. Cao, *Anal. Chem.*, 2018, **90**, 3608–3614.
41 A. K. Mahapatra, S. Mondal, S. K. Manna, K. Maiti, R. Maji, S. S. Ali, S. Mandal, M. Uddin and D. K. Maiti, *ChemistrySelect*, 2016, **1**, 375–383.